Top Organomet Chem (2010) 28: 113–142
DOI: 10.1007/978-3-642-01866-4_4

Luminescent Iridium Complexes and Their Applications

Zhiwei Liu, Zuqiang Bian, and Chunhui Huang

Abstract Considerable studies have been made on iridium complexes during the past 10 years, due to their high quantum efficiency, color tenability, and potential applications in various areas. In this chapter, we review the synthesis, structure, and photophysical properties of luminescent Ir complexes, as well as their applications in organic light-emitting diodes (OLEDs), biological labeling, sensitizers of luminescence, and chemosensors.

Keywords Biological labeling, Chemosensor, Iridium complex, Luminescent, Organic light-emitting diodes, Structure, Synthesis

Contents

Z. Liu, Z. Bian, and C. Huang (✉)
Beijing National Laboratory for Molecular Sciences (BNLMS), State Key Laboratory of Rare Earth Materials Chemistry and Applications, Peking University, Beijing 100871, People's Republic of China
e-mail: chhuang@pku.edu.cn

1 Introduction

There has been growing interest in luminescent iridium (Ir) complexes due to their high quantum efficiency and color tunability. The highly efficient emission is attributed to strong spin-orbit coupling caused by the presence of the 5*d* metal ion, which leads to efficient intersystem crossing from a singlet to a triplet excited state. Mixing of the singlet and triplet excited states via spin-orbit coupling relaxes the spin-forbidden nature of the radiative relaxation of the triplet state [1, 2]. Color diversity arises because excited states in Ir complexes are ligand-related. The energy of the lowest excited state can therefore be controlled by deliberately adjusting the energy of ligand orbitals through substituent effects [3, 4] or by entirely changing the cyclometalated ligand structure [5, 6].

Various cyclometalated Ir complexes have been reported, which can be classified into two main groups. The first group is neutral, containing $Ir(C\hat{}N)_3$ [2, 4, 7–18] (C is a cyclometalated carbon and N is a heterocyclic nitrogen) and $Ir(C\hat{}N)_2(LX)$ [6, 19–28] (LX represents an ancillary ligand) type with tris-bidentate ligands, and $Ir(N\hat{}C\hat{}N)(C\hat{}N\hat{}X)$ (X is an anionic ligand or cyclometalated carbon) [29–31] type with bi–tridentate ligands. The other group is ionic, including $[Ir(C\hat{}N)_2(N\hat{}N)]^+$ [32–40] type with tris-bidentate ligands, $[Ir(C\hat{}N)_2(L)_2]^-$ [41] (L denotes an anionic ancillary ligand) type with unidentate and bidentate ligands, and $[IrN_{6-n}C_n]^{(3-n)+}$ ($n = 0, 1, 2$) [31, 42–44] type with tridentate ligands. Because of their rich photophysical properties, Ir complexes have been widely studied in many applications, such as organic light-emitting diodes (OLEDs) [1, 2, 6, 8, 10, 13, 19, 20, 24, 26, 41, 45–51], light-emitting electrochemical cells (LECs) [52–60], biological labeling [33–36, 61–64], sensitizers of luminescence [65–67], and chemosensors [11, 68–71].

The synthesis, structure, and photophysical properties of luminescent Ir complexes, as well as their applications are introduced in this chapter.

2 Synthesis and Structure

2.1 Neutral Iridium Complex

2.1.1 $Ir(C\hat{}N)_3$ Type

In 1985, Watts et al. reported the first $Ir(C\hat{}N)_3$-type Ir complex *facial*-$Ir(ppy)_3$ (*fac*-**1**), which was formed in 10% yield as a side product in the reaction of Hppy (2-phenylpyridine) with hydrated $IrCl_3$ [16]. They subsequently attempted to extend this procedure with methyl-substituted ppy ligands, but only trace amounts of the desired complex were obtained [4]. In 1991, they developed a new procedure for the high-yield synthesis of *fac*-$Ir(C\hat{}N)_3$ with ppy and other substituted ppy ligands [4]. The procedure utilized the starting material $Ir(acac)_3$ (acac =

2,4-pentanedionate) instead of hydrated $IrCl_3$ (Fig. 1). The method typically produced *fac*-Ir(C^N)$_3$ in high yields of 40–75%, but did not prepare complexes for other structural cyclometalated ligands. To solve this problem, Güdel et al. reported another method in 1994 which involved treating a μ-dichloro bridged dimer complex $[Ir(C^N)_2Cl]_2$ with excess HC^N (free cyclometalated ligand). They found that *fac*-Ir(C^N)$_3$ complexes containing different cyclometalated ligands could be synthesized in high yield [17].

Since the initial report in 1999 using *fac*-**1** as an emitter achieved highly efficient phosphorescent OLEDs, many Ir(C^N)$_3$-type Ir complexes, including small molecular complexes [8, 9, 15] and dendritic complexes [72–78], have been reported. The synthesis and structure of these complexes have been thoroughly investigated.

In general, there are three synthetic methods to prepare Ir(C^N)$_3$-type complexes (Fig. 2). Methods B and C have several advantages over method A. For example, Ir(C^N)$_2$(O^O) (O^O = 2,2,6,6-tetramethyl-3,5-heptanedionate) and $[Ir(C^N)_2Cl]_2$ compounds are easily prepared in high yield from a less expensive starting material; methods B and C give higher yields than method A in the last reaction step [15].

Meridional (abbreviated as *mer*) isomers of Ir(C^N)$_3$ complexes can also be prepared as a different steric geometry configuration of the facial isomers (Fig. 3). Results show that *fac*-Ir(C^N)$_3$ tends to form under higher temperature (suggesting that *fac* isomers are thermodynamically favored products), whereas *mer*-Ir(C^N)$_3$ can be obtained at lower temperature (suggesting that *mer* isomers are kinetically favored products). This is consistent with the experimental phenomenon that the *mer* isomer can be converted to the *fac* isomer under treatment at high temperature [15].

Meridional and *fac* isomers are different not only in steric geometry configuration, but also in Ir–N and Ir–C bond lengths. Key bond lengths of *fac*-Ir(tpy)$_3$ (*fac*-**2**,

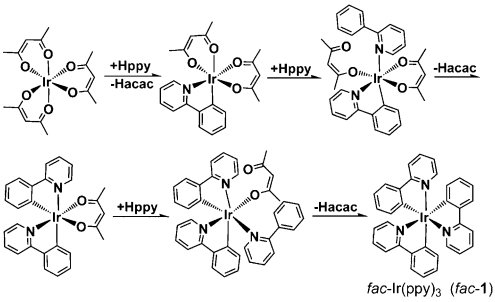

Fig. 1 Schematic representation of the reaction mechanism in the synthesis of Ir(C^N)$_3$ type complex *fac*-**1**

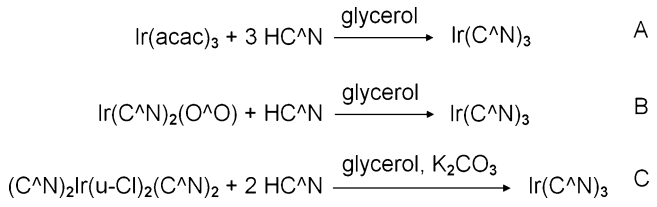

Fig. 2 Three synthetic methods to prepare Ir(C^N)$_3$ type Ir complex

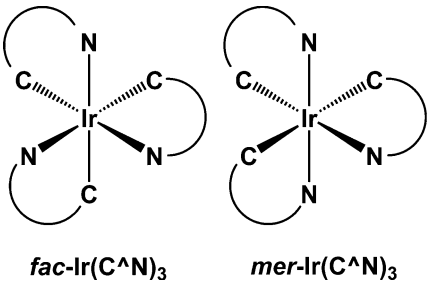

Fig. 3 Steric configuration for *fac*-Ir(C^N)$_3$ and *mer*-Ir(C^N)$_3$

fac- Ir(tpy)$_3$ (*fac*-**2**)

Bond type	Bond length (A)	
	fac-**2**	*mer*-**2**
Ir-N1		2.151(9)
Ir-N2	2.132(5)	2.044(8)
Ir-N3		2.065(8)
Ir-C1		2.076(10)
Ir-C2	2.024(5)	2.086(12)
Ir-C3		2.020(8)

mer- Ir(tpy)$_3$ (*mer*-**2**)

Fig. 4 Crystal structures and key bond lengths of Ir(C^N)$_3$ type Ir complexes *fac*-**2** and *mer*-**2**

tpy is 4-methylphenylpyridine) and *mer*-Ir(tpy)$_3$ (*mer*-**2**) are compared in Fig. 4. In the *fac* isomer, all the Ir–C bonds are *trans* to a pyridyl group, and the Ir–N bonds are *trans* to a phenyl group, leading to identical Ir–C and Ir–N bond lengths. In the *mer* isomer, some of the bond lengths differ markedly from those of the *fac* isomer. This may be because Ir–C (or Ir–N) bonds in the *mer* isomer share an identical/different electronic environment to Ir–C (or Ir–N) bonds in the *fac* isomer.

2.1.2 Ir(C^N)$_2$(LX) Type

The universal synthetic method used to prepare an Ir(C^N)$_2$(LX)-type complex is shown in Fig. 5. Dimer complex [Ir(C^N)$_2$Cl]$_2$ is readily prepared from reaction of the ligand precursor and $IrCl_3 \cdot nH_2O$ [79], and chloro-ion ligands can be subsequently replaced with an LX chelate. The most studied ancillary ligand LX is acac, but it can be varied with other monoanionic bidentate ligands, such as picolinic acid, *N*-methylsalicylimine [23], 2-(5-phenyl-4*H*-[1,2,4]triazol-3-yl)-pyridine [28], 2,2,6,6-tetramethyl-3,5-heptanedionate, 1-phenyl-4,4-dimethyl-1,3-pentanedionate, 1,3-diphenyl-1,3-propanedionate, pyrazolyl, pyrazolyl-borate [80], and (2-pyridyl) pyrazolate derivatives [81].

To understand the structure of the Ir(C^N)$_2$(LX)-type Ir complex, the crystal structure of Ir(tpy)$_2$(acac) (**3**, Fig. 6) was compared with *fac*-**2** and *mer*-**2** mentioned above. The bis-cyclometalated fragment of **3** has the same disposition of tpy ligands

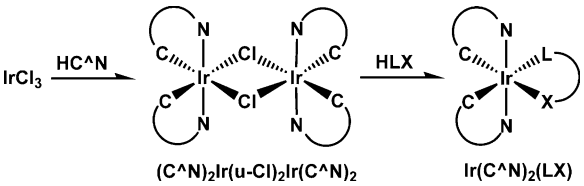

Fig. 5 Synthetic route for $Ir(C^N)_2(LX)$ type complex

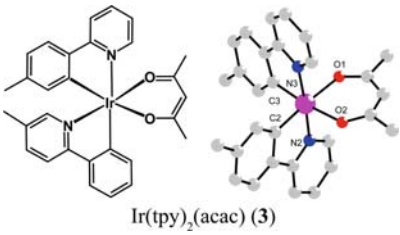

Fig. 6 Chemical and crystal structures of $Ir(C^N)_2(LX)$ type complex **3**

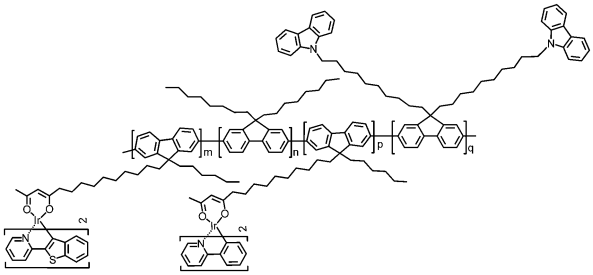

Fig. 7 Chemical structure of a polymerized $Ir(C^N)_2(LX)$-type Ir complex

as found in *mer*-**2**, and the mutually *trans*-disposed Ir–N bonds in both complexes have similar lengths (av = 2.032(5) Å). The weak *trans* influence of the acac ligand leads to shorter Ir–C bonds (av = 1.984(6) Å) for the complex **3** than those observed in complex *fac*-**2** or *mer*-**2**.

There is also a polymerized $Ir(C^N)_2(LX)$-type Ir complex in which the bis-cyclometalated fragment $Ir(C^N)_2$ is incorporated on the side chain of a polymer. The design of the entire system could have better dissolution and film-forming ability as that of the polymer, as well as high quantum efficiency similar to that of luminescent Ir complexes. The chemical structure of a selected polymerized $Ir(C^N)_2(LX)$-type Ir complex is shown in Fig. 7 [82].

2.1.3 Ir(N^C^N)(C^N^X) Type

Neutral Ir complexes mentioned above are all composed of bidentate ligands. Believing tridentate ligands can lead to different excited state, stereoisomer, and

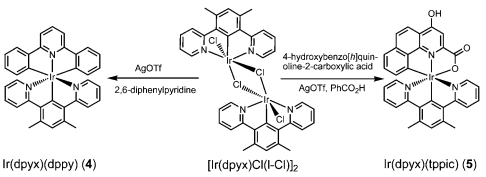

Fig. 8 Synthetic methods of Ir(N^C^N)(C^N^X) type complexes **4** and **5**

linear assembly, some groups focused their research on Ir complex with tridentate ligands. Figure 8 shows the synthetic methods of Ir(dpyx)(dppy) (**4**) and Ir(dpyx)(tppic) (**5**), two neutral Ir complexes with tridentate ligands. Complex **4** was obtained by heating the chloro-bridged dimer $[Ir(dpyx)Cl(l\text{-}Cl)]_2$ with AgOTf in molten 2,6-diphenylpyridine (dppyH), followed by rapid chromatographic purification [30], while complex **5** was synthesized upon reaction of the dimer with 4-hydroxybenzo[*h*]quinoline-2-carboxylic acid (tppicH) using molten benzoic acid as the solvent [29]. The N^C^N tridentate coordination mode of dpyx was confirmed in $[Ir(dpyx)\text{-}(DMSO)Cl_2]$ (DMSO is dimethyl sulfoxide) by X-ray crystal structure [29].

2.2 Ionic Iridium Complex

2.2.1 $[Ir(C^N)_2(N^N)]^+$ Type

The cyclometalated Ir complexes investigated earlier with a formula of $[Ir(C^N)_2(N^N)]^+$ are complexes $[Ir(ppy)_2(bpy)]Cl$ (**6**) and $[Ir(ppy)_2(bpy)]PF_6$ (**7**) (bpy and PF_6 represent 2,2′-bipyridine and hexafluorophosphate, respectively) [39]. The two cationic Ir complexes were prepared by a modified method employed by Nonoyama [83]. The detailed synthetic route is shown in Fig. 9. The stereo structure of these $[Ir(C^N)_2(N^N)]^+$ complexes is similar to those of $Ir(C^N)_2(LX)$ complexes, with a *trans-N,N* configuration of the C^N ligands, whereas the diimine ligand is located opposite *cis*-oriented carbon atoms, completing an octahedral arrangement [84].

2.2.2 $[Ir(C^N)_2(L)_2]^-$ Type

An $[Ir(C^N)_2(L)_2]^-$ type anionic Ir complex can be conveniently synthesized in low-boiling solvent by reacting the corresponding $[Ir(C^N)_2Cl]_2$ dimer complex with a pseudohalogen ligand such as tetrabutylammonium cyanide, tetrabutylammonium thiocyanate, or tetrabutylammonium cyanate [41, 85]. Figure 10 shows the chemical and crystal structure of the complex $(C_4H_9)_4N[Ir(ppy)_2(CN)_2]$ (**8**) [41, 85]. The Ir atom is octahedrally coordinated by four ligands, with the N atoms of the

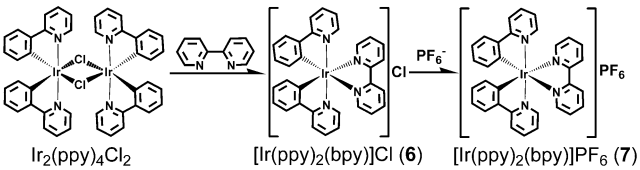

Fig. 9 Synthetic route to $[Ir(C^N)_2(N^N)]^+$ type complexes **6** and **7**

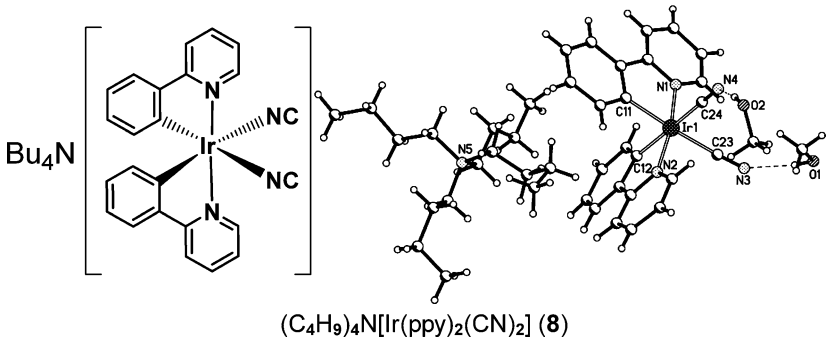

Fig. 10 Chemical and crystal structures of $[Ir(C^N)_2(L)_2]^-$ type complex **8**

2-phenylpyridine ligands in a *trans* disposition similar to that in $[Ir(ppy)_2Cl]_2$, whereas cyanide ligands coordinate through the carbon atom and adopt a *cis* configuration.

These complexes are stable at room temperature as a solid and in solution containing noncoordinating solvents such as dichloromethane, chloroform, methanol, or ethanol. This type of Ir complex may undergo slow substitution of the pseudohalogen ligands upon standing for days in a strong coordinating solvent such as dimethyl sulfoxide [41].

2.2.3 $[IrN_{6-n}C_n]^{(3-n)+}$ (n = 0, 1, 2) Type

Figure 11 shows chemical structures for $[IrN_{6-n}C_n]^{(3-n)+}$ (n = 0, 1, 2) type Ir complexes with tridentate ligands. Complex **9** was first reported by Degraff and coworkers, with fusion reaction and arduous purification [86]. Subsequently, a milder and stepwise route was described by Sauvage, involving initial reaction of terpyridine (tpyH) with $IrCl_3 \cdot nH_2O$ in ethylene glycol to give $[Ir(tpy)Cl_3]$ as an intermediate, followed by reaction with a second equivalent of tpy in refluxing ethylene glycol [87]. Purification of the tricationic complex is normally best achieved after ion exchange to the hexafluorophosphate salt, which offers the advantage of being soluble in polar organic solvents for column chromatography [31]. In order to obtain complexes **10** and **11**, compound 1,3-di(2-pyridyl)-4,6-dimethylbenzene (dpyxH) was employed to react with $IrCl_3 \cdot nH_2O$ to give a chloro-bridged dimer $[Ir(dpyx)Cl(\mu\text{-}Cl)]_2$, reactions of the dimer with 4′-tolylterpyridine (tppyH) and 6-phenyl-2,2′-bipyridine (phbpyH)

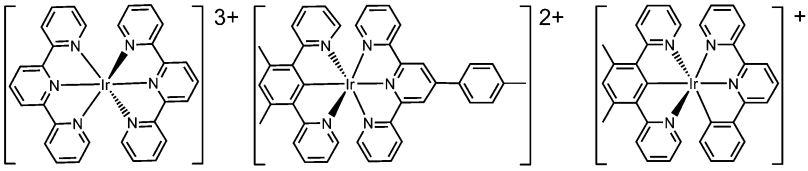

Fig. 11 Chemical structures of $[IrN_{6-n}C_n]^{(3-n)+}$ ($n = 0, 1, 2$) type complexes **9–11**

gives complex **10** and **11**, respectively [29, 30]. An X-ray diffraction study of a single crystal of the former confirms the mutually orthogonal orientation of the two ligands, each bound tridentately [30].

3 Photophysical Properties

3.1 Neutral Iridium Complex

3.1.1 $Ir(C^N)_3$ Type

The photophysical properties of $Ir(C^N)_3$ have been examined by several research groups [8, 15]. Two principal transitions are observed in this type of Ir complex: (1) metal-to-ligand charge transfer (MLCT) in which an electron is promoted from a metal *d* orbital to a vacant π* orbital on one of the ligands and (2) ligand-centered (LC) transitions in which an electron is promoted between π orbitals on one of the coordinated ligands. Phosphorescence in $Ir(C^N)_3$-type complexes enabled by strong spin-orbit coupling mainly arise from a mixture of ^{3}LC and ^{3}MLCT excited states, whereas the emissive excited state is predominantly the excited state having the lowest energy.

The lowest excited state of a $Ir(C^N)_3$-type complex can be tuned by changing the substitution of electron-donating or electron-withdrawing groups on the cyclometalated ligand, or by entirely changing the cyclometalated ligand structure [15]. Table 1 lists the photophysical properties of complexes **1** (Fig. 1), **2** (Fig. 4), $Ir(46dfppy)_3$ (**12**), $Ir(ppz)_3$ (**13**), $Ir(46dfppz)_3$ (**14**), and $Ir(tmfppz)_3$ (**15**) (Fig. 12). Photophysical properties of complex **2** (**14**) are different from that of **12** (**15**), but both are similar to those of parent compound **1** (**13**). This is unsurprising because substitution of donor or acceptor groups tunes the highest occupied molecular orbital (HOMO) and the lowest unoccupied molecular orbital (LUMO) levels of the metal complex in parallel, leading to marginal changes in maximal emission. Photophysical properties of complex **13** are entirely changed compared with complex **1**, which is ascribed to skeletal change of the cyclometalated ligand.

Table 1 Photophysical properties of complexes **1**, **2**, **12**–**15** in 2-methyltetrahydrofuran

Complex	Emission at 77 K		Emission at 298 K		
	λ_{max}	τ (μs)	λ_{max}	τ (μs)	Φ_{PL}
fac-**1**	492	3.6	510	1.9	0.40
Mer-**1**	493	4.2	512	0.15	0.036
fac-**2**	492	3.0	510	2.0	0.50
Mer-**2**	530	4.8	550	0.26	0.051
fac-**12**	450	2.5	468	1.6	0.43
Mer-**12**	460	5.4	482	0.21	0.053
fac-**13**	414	14	–	–	–
mer-**13**	427	28	–	–	–
fac-**14**	390	27	–	–	–
mer-**14**	402	33	–	–	–
fac-**15**	422	17	428	0.05	–
mer-**15**	430	32	–	–	–

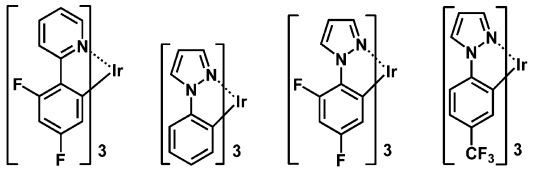

Ir(46dfppy)$_3$ (**12**) Ir(ppz)$_3$ (**13**) Ir(46dfppz)$_3$ (**14**) Ir(tmfppz)$_3$ (**15**)

Fig. 12 Chemical structures of complexes **12**–**15**

Photophysical properties of *mer*-Ir(C^N)$_3$-type complexes are very different to those of *fac*-Ir(C^N)$_3$-type complexes (Table 1). Meridional ones traditionally exhibit a broad, red-shifted emission, and lower quantum efficiencies, which can be attributed to the reason that the *mer* configuration usually arises from strongly *trans* influencing phenyl groups being opposite each other [88].

3.1.2 Ir(C^N)$_2$(LX) Type

The lowest triplet energy level of the ancillary ligand LX lie well above the energies of LC and MLCT excited states in most of the Ir(C^N)$_2$(LX)-type complexes, so luminescence of Ir(C^N)$_2$(LX) is dominated by ^{3}LC and ^{3}MLCT transitions. This leads to similar phosphorescence emission to the *fac*-Ir(C^N)$_3$ complexes with the same cyclometalated ligand [6, 23]. In such cases, density functional theory (DFT) calculations indicate that HOMOs are largely metal-centered, whereas LUMOs are primarily localized on the heterocyclic rings of the cyclometalated ligand. The ancillary is therefore not directly involved in the lowest excited state.

Though the ancillary ligand is not directly involved in the lowest energy excited state when it has a higher triplet energy level, it can alter the excited energy state by modifying electron density at the metal center [80]. Figure 13 shows the emission spectra of Ir(tpy)$_2$(pz$_2$Bpz$_2$) (**16**), Ir(tpy)$_2$(pz$_2$H) (**17**), Ir(tpy)$_2$(pzH)Cl (**18**), and Ir(tpy)$_2$(acac) (**3**) at room temperature. All have the same "Ir(tpy)$_2$" fragment, but there is a clear blue-shift in the maximum emission wavelength as the ancillary

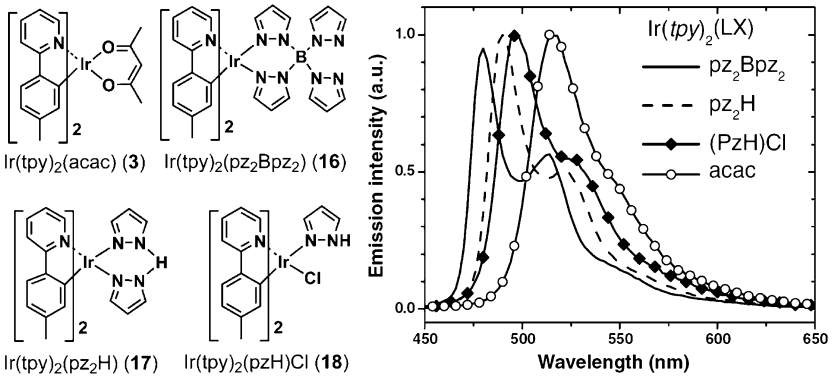

Fig. 13 Chemical structures of **16–18**, and their photoluminescent spectra in 2-methyltetrahydrofuran compared with **3** at room temperature

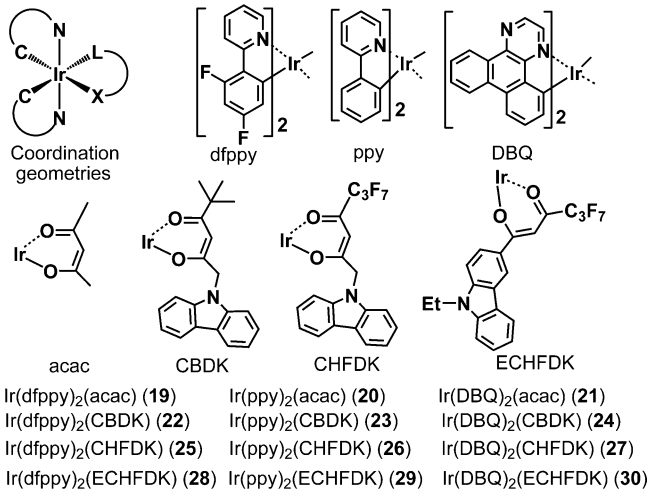

Fig. 14 Chemical structures of complexes **19–30**

ligand is changed. This is attributed to a net electron-withdrawing ancillary ligand that pulls electron density away from the Ir atom, thereby stabilizing the metal orbitals and lowering the HOMO energy; whereas the LUMO of the $Ir(tpy)_2(LX)$ complexes, localized on the pyridyl rings, is expected to be largely unaffected with respect to energy. The HOMO-LUMO gap should consequently increase for stronger electron-withdrawing ancillary ligands, leading to a blue-shift in emission.

If the lowest triplet energy level of the LX ligand is lower in energy than the ^{3}LC or ^{3}MLCT, it will be the lowest energy excited state, and thus a switch from "$Ir(C\text{^}N)_2$" to LX-based emission can be observed. Our recent work confirms this hypothesis [89]. Twelve Ir complexes (complexes **19–30**, Fig. 14) with general formula $Ir(C\text{^}N)_2(LX)$ were synthesized by changing the triplet energy level of the

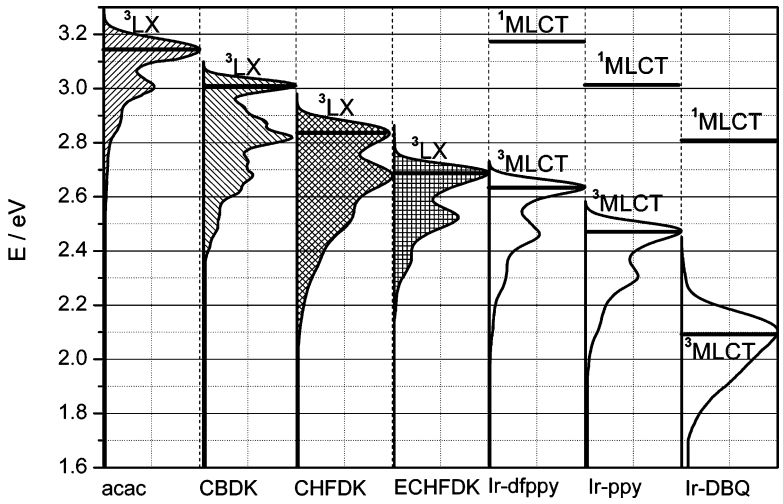

Fig. 15 State density of triplet energy diagram for the β-diketonates and $Ir(C^N)_2$ fragments of complexes **19–30**

cyclometalated and the β-diketonate ligands, and photophysical properties were compared. Strong ^{3}LC- or ^{3}MLCT-based phosphorescence was observed if triplet-state density maps of the β-diketonate and the $Ir(C^N)_2$ fragment were not superimposed (triplet energy of the former is high). If the triplet-state density map of the two parts was superimposed, ^{3}LC- or ^{3}MLCT-based transition would be quenched at room temperature, and DFT calculations show that the lowest excited state is determined by the cyclometalated and ancillary ligand (Fig. 15).

Interligand electron transfer (ILET) from the cyclometalated ligand to the ancillary ligand is also possible in some excited $Ir(C^N)_2(LX)$ complexes, particularly if the triplet energy of the ancillary ligand is much lower. Park et al. observed emission across the visible spectrum by changing the structure of the ancillary ligand in a series of complexes undergoing ILET before emission [90–92].

3.2 Ionic Iridium Complex

3.2.1 $[Ir(C^N)_2(N^N)]^+$ Type

The photophysical properties of $[Ir(C^N)_2(N^N)]^+$-type cationic Ir complexes are complicated. In some excited complexes, the neutral, diimine and cyclometalated ligands provide orbitals that participate in excited-state transitions. The cyclometalated ligand tends to be associated with the ^{3}LC transition, and the diimine ligand with the ^{3}MLCT transition [93]. In such cases, the excited state of the complex can be tuned directly through ligand modification because each ligand is linked to a

different transition. Nazeeruddin et al. investigated three cationic Ir complexes **31**–**33** (Fig. 16) by modulating the electronic structure of the complex using selective ligand functionalization [94]. They developed a strategy to tune the phosphorescence wavelength for this class of compound [94]. The electron-withdrawing substituent on the C^N ligand decreased donation to the metal and therefore stabilized the metal-based HOMO, whereas the electron-releasing substituent on the N^N ligand led to destabilization of the N^N ligand-based LUMO, ultimately leading to increased HOMO-LUMO gaps and emission energies (Table 2).

It was proved that photophysical properties of $[Ir(C^N)_2(N^N)]^+$-type complexes can also be adjusted by modifying the conjugated lengths of the diimine ligand [84]. Theoretical calculations, photophysical studies and electrochemical studies of a series of cationic Ir complexes **34**–**39** (Fig. 17) showed that their excited

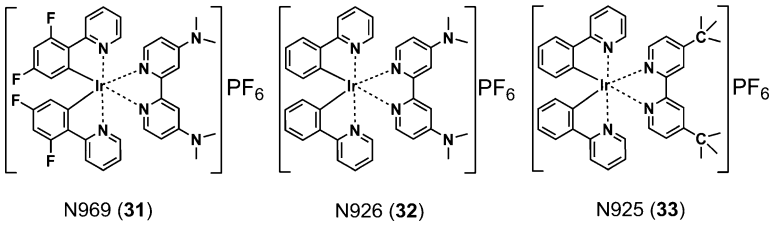

Fig. 16 Chemical structures of **31**–**33**

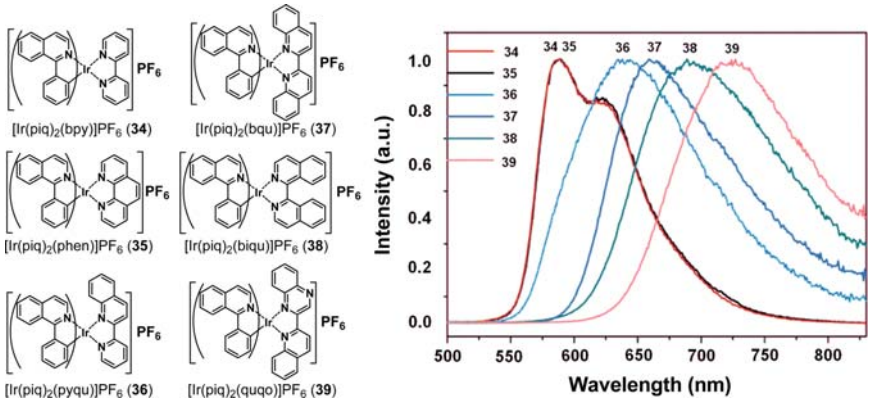

Fig. 17 Chemical structures and emission spectra of **34**–**39**

Table 2 Photophysical properties of complexes **31**–**33** in acetonitrile at 298 K

Complex	λ_{max}	Φ_{PL}	τ (μs)
31	463, 493	0.85 ± 0.1	4.11 ± 0.02
32	491, 520	0.80 ± 0.1	2.43 ± 0.02
33	581	0.23	0.557

states simultaneously contain ^{3}MLCT, triplet ligand-to-ligand charge transfer (^{3}LLCT), and ^{3}LC transitions. Their emission wavelengths can therefore be tuned significantly (~150 nm) by changing the conjugated length of N^N ligands.

3.2.2 $[Ir(C^N)_2(L)_2]^-$ Type

The structures of cyclometalated ligand C^N and spectator ligand L should be considered when evaluating the photophysical properties of $[Ir(C^N)_2(L)_2]^-$-type Ir complexes. By keeping the cyclometalated ligand C^N as 2-phenylpyridine, Nazeeruddin et al. introduced three pseudohalogens, CN^-, NCS^-, and NCO^-, as spectator ligand L [41]. They investigated the influence of the spectator ligand on the photoluminescent properties of this type of complex {$(C_4H_9)_4N[Ir(ppy)_2(CN)_2]$, complex **8** in Fig. 10; $(C_4H_9)_4N[Ir(ppy)_2(SCN)_2]$, complex **40**, and $(C_4H_9)_4N[Ir(ppy)_2(OCN)_2]$, complex **41**, in Fig. 18)} in 2003 [41]. Introducing a strong ligand field strength spectator ligand such as CN^- increased the gap between LUMO of the phenyl pyridine ligand and metal t_{2g} orbitals, resulting in a blue-shift in the emission spectrum. The gap between the LUMO of the phenyl pyidine ligand and the vacant metal e_g orbitals effectively increased because of the inhibition of nonradiative pathways by the cyanide ligands, which also led to these complexes displaying unusually high phosphorescence quantum yields in solution at room temperature.

While maintaining the spectator ligand L as CN^-, Nazeeruddin et al. traced the effect of cyclometalated ligands (**8** in Fig. 10; **42**–**45** in Fig. 18) in 2008 [85]. They found that introduction of 4-dimethylaminopyridine can destabilize LUMO and HOMO orbitals in parallel, leading to marginal changes in emission spectra, but it increased nonradiative rate constants, which in turn led to a reduction of overall quantum yield. They also found that introducing fluorine atoms on the phenyl

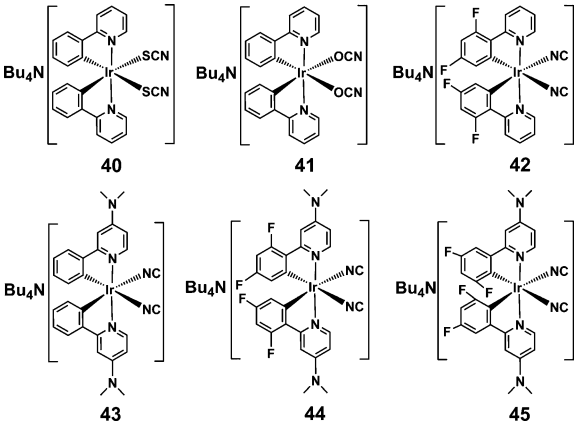

Fig. 18 Chemical structures of complexes **40**–**45**

Table 3 Photophysical properties of complexes **8** and **40–45** in acetonitrile solution at 298 K

Complex	λ_{max}	Φ_{PL}	τ (μs)
8	470, 502	0.94 ± 0.05	3.14 ± 0.5%
40	506, 520	0.97 ± 0.05	1.43 ± 0.5%
41	538, 560	0.99 ± 0.05	0.85 ± 0.5%
42	460, 485	0.80 ± 0.1	3.28 ± 0.03
43	465, 488, 525sh	0.54 ± 0.1	1.82 ± 0.03
44	451, 471, 525sh	0.62 ± 0.1	1.30 ± 0.03
45	468, 492	0.64 ± 0.1	3.00 ± 0.03

groups led to stabilization of HOMO orbitals. This led to an increase in the HOMO-LUMO gap and was accompanied by a blue-shift in emission spectra, but it did not substantially influence quantum yields because of a slight increase in radiative rate constants or a decrease in overall nonradiative rate constants. Based on these findings, they provided an interesting approach for tuning the phosphorescence wavelength from 470 to 450 nm of anionic Ir complexes, maintaining a high phosphorescence quantum yield by modification with donor and acceptor substituents on the pyridine and phenyl moieties of 2-phenylpyridine (detailed photophysical data are summarized in Table 3).

The photophysical properties of both neutral Ir(N^C^N)(C^N^X) type and ionic $[IrN_{6-n}C_n]^{(3-n)+}(n = 0, 1, 2)$ type Ir complexes with tridentate ligands, in particular how the number of cyclometalating carbon atoms in the coordination sphere of the metal ion influences the luminescence, were comprehensively reviewed by Williams in 2008 [31].

4 Applications of Luminescent Iridium Complexes

4.1 Applications in OLEDs

OLEDs are electroluminescent devices in which electrical energy is converted to luminous energy. A typical configuration is depicted in Fig. 19. Two electrodes sandwich one or more layers of the organic functional films. A voltage of 2–10 V is typically applied between the electrodes, and electrons are injected into the LUMO of the organic material from a low work function metallic cathode such as Mg–Ag or Li–Al. Holes are injected into the HOMO of the organic material from a high work function anode such as indium–tin–oxide (ITO). Electrons and holes move towards the middle region of the emitting layer under the influence of the applied field. Energetic electrons can drop into the holes to form singlet and triplet excitons which release their energy as photons escaping through the transparent electrode.

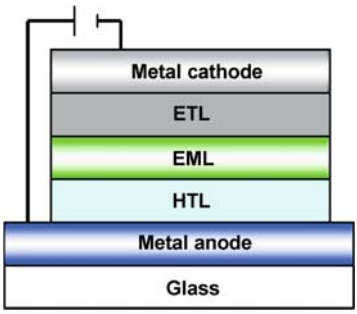

Fig. 19 Typical configuration of OLEDs, ETL: electron-transporting layer; EML: emitting layer; HTL: hole-transporting layer

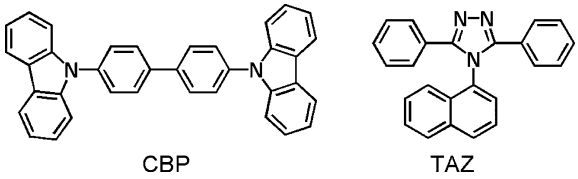

Fig. 20 Chemical structures of CBP and TAZ

4.1.1 Emitters for Doping OLEDs

Ir complexes have been doped into a charge-transporting host material to optimize device efficiency up to a theoretical limit. The remarkable enhancement in efficiency upon doping has been ascribed to a favorable triplet energy level alignment between host material and Ir complex dopant. Triplet–triplet annihilation, which is a key adverse factor for phosphorescence-based emitters, can also be greatly inhibited by dispersing emitter molecules into the host matrix. Highly efficient red, green, blue (RGB) devices (which are necessary for full-color displays) can be explored by doping different color emission Ir complexes into an appropriate host.

Green-phosphorescent OLED is the best developed RGB device. Cyclometalated *fac*-**1** and its heteroleptic analog such as $Ir(ppy)_2(acac)$ (**20** in Fig. 14) have been extensively applied in fabricating green-emitting electroluminescent devices. In 1999, Forrest et al. described high-efficiency OLEDs employing *fac*-**1** as the dopant and CBP (Fig. 20) as the host [2]. The combination of a short triplet lifetime and reasonable photoluminescent efficiency allows *fac*-**1** based OLEDs to achieve peak quantum efficiencies of 8.0%. In 2000 they demonstrated much higher efficiency OLEDs by doping *fac*-**1** into an electron-transport layer host TAZ (Fig. 20) [10]. A maximum external quantum efficiency of 15.4 ± 0.2% was achieved. In 2001, they again demonstrated very high efficiency OLEDs employing **15** doped into TAZ host [20]. A maximum external quantum efficiency of 19.0 ± 1.0% was achieved. The calculated internal quantum efficiency of 87 ± 7% is supported by the observed absence of thermally activated nonradiative loss in the photoluminescent efficiency of **20**. Very high external quantum efficiencies are therefore due to the nearly 100% internal phosphorescence efficiency of the Ir complex coupled

with balanced hole and electron injection, as well as triplet exciton confinement within the light-emitting layer.

Compared to green OLEDs, development of red OLEDs has been slower. This is because red emission originated from a smaller energy gap transition, which increased the difficulty of material searching. Many nonradiative pathways originating from strong π–π interaction or charge transfer between ligands may be present, leading to a reduction in efficiency in the OLEDs. The earliest report concerning a red emitting Ir complex as an emitter was by Forrest et al. in 2001 [19]. The device achieved a maximum external quantum efficiency of 7.0 ± 0.5% using a red phosphor $Btp_2Ir(acac)$ (**46**, Fig. 21) as the dopant and CBP as the host. In 2003, Tsuboyama et al. fabricated an efficient red OLED device using a novel Ir emitter $Ir(piq)_3$ (**47**, Fig. 21) as a dopant [8]. The maximum external quantum efficiency was 10.3%. Duan et al. synthesized two new orange–red Ir complexes, $Ir(DBQ)_2(acac)$ (**21**, Fig. 14) and $Ir(MDQ)_2(acac)$ (**48**, Fig. 21) [24]. The devices based on these two complexes emit orange–red light, and the maximum external quantum efficiency is 12%.

Highly efficient blue OLEDs are necessary to realize RGB full-color displays. One of the best known phosphorescence blue emitters is FIrpic (**49**, Fig. 22) [95]. A maximum external electroluminescent quantum efficiency of 7.5 ± 0.8% was obtained by doping **49** into mCP (Fig. 23). The result represents a significant increase in efficiency over a similar device structure based on the host CBP, where the maximum external quantum efficiency was 6.1 ± 0.6%. Data mentioned above indicate that the energy differences in the triplet energies of host and guest materials are very important for confinement of electro-generated triplet excitons on dopant molecules, thus the key factor to achieve highly efficient blue OLEDs is to find appropriate guest and host materials. Based on this guidance, Thompson et al.

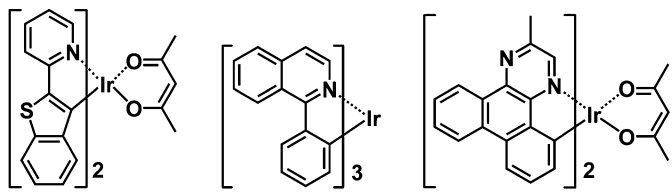

Fig. 21 Chemical structure of red emitters **46–48**

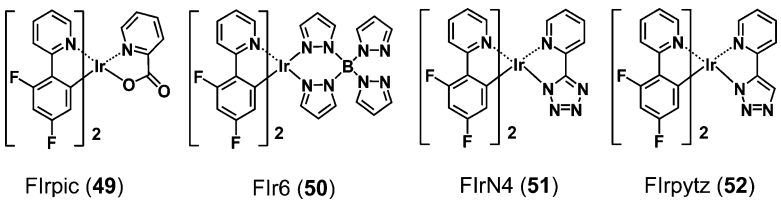

Fig. 22 Chemical structures of blue emitters **49–52**

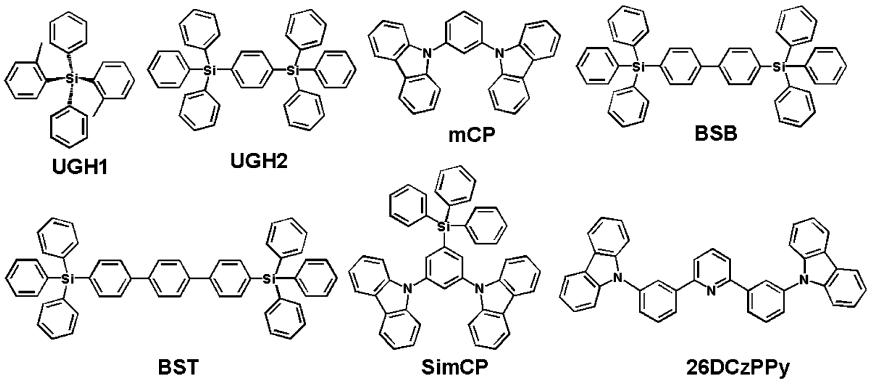

Fig. 23 Chemical structures of some host materials for blue emission iridium complex

demonstrated efficient, deep-blue OLEDs using a charge-trapping phosphorescent guest FIr6 (**50**, Fig. 22) doped in the wide-energy-gap hosts UGH1 and UGH2 (Fig. 23) [25]. Peak quantum efficiencies of 8.8 ± 0.9% in UGH1 and 11.6 ± 1.2% in UGH2 were obtained. In 2005, Yeh et al. reported a series of OLEDs based on FIrN4 (**51**, Fig. 22) or **49** dopant emitters coevaporated with mCP or SimCP (Fig. 23) [48]. The device based on **51** and mCP was found to be one of the bluest OLEDs. The device based on **49** and SimCP achieved maximum external electroluminescent quantum efficiency of 14.4%. Considering UGH1 and UGH2 are less conductive compared with the carbazole derivatives, and that the glass transition temperatures of these two compounds are low for practical application, Lin et al. synthesized two hosts, BSB and BST (Fig. 23), as well as a new blue Ir complex FIrpytz (**52**, Fig. 22) [96]. By using BSB as the host for the blue emitter **52**, highly efficient blue OLEDs with external quantum efficiency of 19.3% was achieved. Su et al. recently reported a unique molecular design strategy of combining a carbazole electron donor with a high triplet energy and a pyridine electron acceptor with high electron affinity to give a novel bipolar host material of 26DCzPPy (Fig. 23) [97]. By using the host for **49**-based blue phosphorescent OLEDs, an external quantum efficiency of 24% was achieved at the practical brightness of 100 cd m^{-2}. Even at a brighter emission of 1,000 cd m^{-2}, an efficiency of 22% was obtained.

Despite the investigation of RGB OLEDs for display applications, Ir complexes have also been used to exploit near-infrared (NIR) OLEDs for optical communication and biomedical application. Jabbour et al. demonstrated the first example of NIR OLEDs fabricated by the cyclometalated Ir complex NIR1 (**53**, Fig. 24) by increasing the size of the cyclometalated ligand π system [98]. The devices exhibited exclusive emission with a peak value at 720 nm, and the external quantum efficiency was nearly 0.1%.

Ir complexes were also used to develop white OLEDs (WOLEDs) for large-scale production of solid-state light sources and backlights in liquid-crystal displays. Several device architectures have been introduced to achieve high brightness and efficiency in WOLEDs. By controlling the recombination current within individual

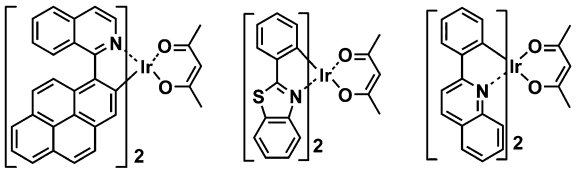

Fig. 24 Chemical structures of **53–55**

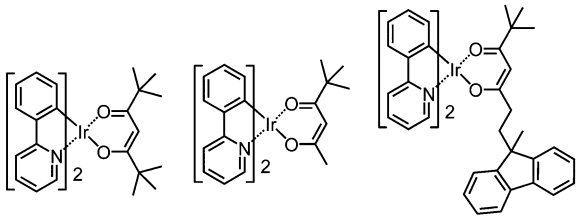

Fig. 25 Chemical structures of **56–58**

organic layers, emission from red **46**, yellow **54** (Fig. 24), and blue **49** was balanced to obtain white of the desired color purity [99]. The most significant disadvantage of this structure is its relatively high operating voltage due to the combined thicknesses of the many layers used in the emission region. To solve this problem, Forrest et al. mixed red **55** (Fig. 24), green *fac*-**1**, and blue **50** into a wide energy gap UGH2 host to ensure that all emission originates from a single thin layer. The process of direct triplet exciton formation of the **50**-UGH2 system leads to a reduction in operating voltage, and hence an increase in power efficiency up to 42 ± 4 lm W^{-1} was obtained [100].

Doping OLEDs mentioned above are all using fluorescent materials as the host material. Phosphorescent materials can also be used as host material and their performances appear to be significant [50, 101]. Our results proved that highly efficient phosphorescent OLEDs can be pursued using Ir complexes as the host materials [102]. In detail, six devices using **20**, **23** (Fig. 14), **56**, **57** and **58** (Fig. 25) or CBP as the host for an orange–red Ir complex **21** (Fig. 14) were fabricated with an identical configuration. Results show that the devices using Ir complex hosts had better performances than that of the device based on a CBP host. In addition, steric hindrance and exciton-transporting ability of the host were found to be the most important factors for this type of doped system.

4.1.2 Emitters for Non-doped OLEDs

Up to now, most positive results based on Ir complex emitters have been obtained by using a host–guest doped emitter system to improve energy transfer and to avoid

triplet–triplet annihilation which occurs when phosphorescent materials are used in OLEDs. Considering that reproducibility of the optimum doping level requires careful manufacturing control, and that long-playing operation of devices may lead to phase separation of guest and host materials, doped OLEDs are relatively more difficult to adapt to practical application than their nondoped counterparts [103]. High-performance phosphorescent OLEDs fabricated by a much simplified, nondoped method are rarely studied, and their typical performances with respect to brightness and efficiency are far from satisfactory [13, 25, 104, 105]. It is therefore desirable to design nondoped electrophosphorescent devices with high brightness and efficiency.

A novel red phosphorescent Ir complex containing carbazole-functionalized β-diketonate **24** (Fig. 14) was designed, synthesized, and characterized in our earlier report [106]. Electrophosphorescent properties of a nondoped device using complex **24** as emitter were examined. The nondoped device achieved maximum lumen efficiency of 3.49 lm W^{-1}. This excellent performance can be attributed mainly to the improved hole-transporting property that benefits exciton transportation. Encouraged by the fact that functionalized β-diketonate can have such an important role in the Ir complex, and with a wish to design high-efficiency nondoped green and blue OLEDs, we synthesized two complexes both containing carbazole-functionalized β-diketonate, **22** and **23**, and subsequently fabricated nondoped devices using these two complexes [107]. Lumen efficiency of the green emission device using **23** as emitter was 4.54 lm W^{-1}, whereas the device based on a blue–green **22** achieved maximum lumen efficiency of 0.51 lm W^{-1}. A very simple device and two double-layer devices **23** were also fabricated, and the designed Ir complex was proved to be with good hole-transporting ability and electron-transporting ability. This study provided a special type of doping technology that should have a more general use in emitter design.

As opposed to neutral Ir complexes, charged Ir complexes are mainly synthesized to develop LECs (another type of OLED) [55, 59, 108–110]. In these devices, electrons and holes injected from two air-stable electrodes into a single layer of organic semiconductor recombine, giving rise to light emission. LECs have advantages over traditional OLEDs: (1) LECs require only a single layer of organic semiconductor, whereas traditional OLEDs require a multilayered structure for charge injection, transport, and light emission, and (2) charge injection in an LEC is insensitive to the work function of the electrode material, thereby permitting use with a wide variety of metals as cathode materials. These suggest that LECs may be a promising alternative for solid-state lighting technologies.

4.2 Biological Labeling Reagents

To investigate the potential of luminescent Ir complexes as biological labeling reagents, Lo et al. [33–36, 61–63] reported a series of $[Ir(C\hat{}N)_2(N\hat{}N–R)](PF_6)$

(R = CHO, NCS and $NHCOCH_2I$) complexes incorporating aldehyde, isothiocyanate, and iodoacetamide groups in the ligands. These Ir complexes can be functionalized as biological labeling reagents due to their ability – covalently or noncovalently – to bind biomolecules. Crosslinked products showed different emission colors than

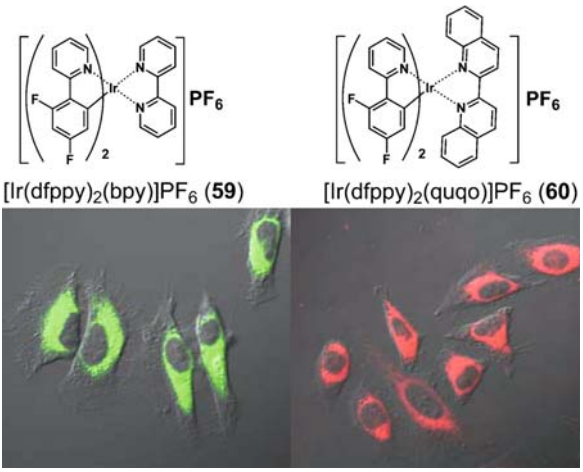

Fig. 26 Chemical structures of **59**, **60**, and their bio-imaging application

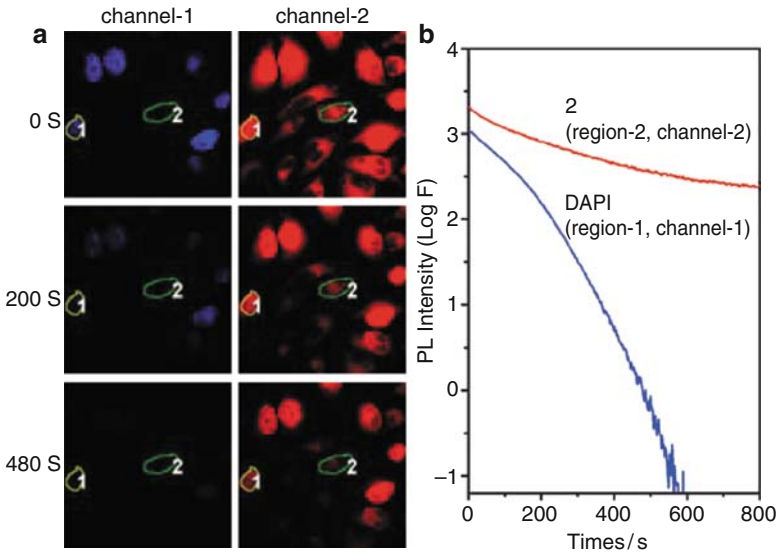

Fig. 27 Comparison of **60** and DAPI for resistance to photobleaching. (**a**) Confocal luminescence images of fixed HeLa cells stained with **60** and DAPI under continuous excitation at 405 nm with different laser scan times (0, 200, 480 s). (**b**) Luminescence decay curves of **60** and DAPI during the same period. The signals of DAPI and **60** were collected from region 1 of channel 1 (460 ± 20 nm) and region 2 of channel 2 (620 ± 20 nm), respectively

their free analogs due to the more hydrophobic environment associated with the protein molecule. A comprehensive review of luminescent Ir complexes used as biological labeling reagents was reported by Lo et al. in 2005 [64].

We recently reported two cationic Ir complexes, **59** (Fig. 26) with bright green emission, and **60** (Fig. 26) with red emission, as phosphorescent dyes for imaging of living cells [111]. These two Ir complexes have advantages when used as bio-imaging agents: exclusive staining in cytoplasm, low cytotoxicity, reduced photo-bleaching, permeability to cell membranes, and moderate luminescence efficiencies in buffer solution.

As shown in Fig. 27, after continuous excitation at 405 nm for 480 s, luminescence intensity of 4′,6′-diamidino-2-phenylindole dihydrochloride (DAPI) (460 ± 20 nm, region 1, channel 1) decreased to 1% of its initial value (owing to photobleaching). Luminescence intensity of **60** (620 ± 20 nm, region 2, channel 2) stayed at essentially one-eighth of the original value during the same period of excitation. This result establishes that the Ir complex show reduced photobleaching and higher photostability than the organic dye. These findings open-up interesting possibilities for using luminescent Ir complexes for imaging of living cells. Investigation of other Ir complexes used in this field will be published in a forthcoming article.

4.3 Sensitizer of Lanthanide Luminescence

Lanthanide ions such as europium (Eu^{III}), neodymium (Nd^{III}), ytterbium (Yb^{III}), and erbium (Er^{III}) are becoming increasingly important in applications such as OLEDs [112–115], optical communication [116, 117], medical imaging, and biological labeling [118, 119] due to their excellent luminescence properties originating from *f–f* transitions. These ions show little or no absorption in the visible region of the spectrum, and often require application of strongly absorbing "antennae" for light harvesting to obtain efficient photoluminescence [120]. Many organic chromophores having high absorbing ability were therefore introduced into lanthanide complexes. The use of strongly-absorbing *d*-block chromophores (e.g., Ir complexes) as sensitizers has attracted increasing attention [65–67].

The first example of sensitization of Eu^{III} emission through an Ir complex was reported by De Cola et al. in 2005 (Fig. 28) [67]. Energy transfer from the Ir fragments to the Eu^{III} center is incomplete, leading to emission of a composite white light instead of Eu^{III}-based emission of pure red light.

To make energy transfer more efficient and obtain pure-red emission from Eu^{III}, a novel ligand with four coordination sites was designed as a bridge to link the Ir^{III} center and the Eu^{III} center; and a new Ir^{III} complex $Ir(dfppy)_2(phen5f)$ [dfppy represents 2-(4′,6′-difluorophenyl)-pyridinato-N,$C^{2\prime}$, phen5f denotes 4,4,5,5,5-pentafluoro-1-(1′,10′-phenanthrolin-2′-yl)-pentane-1,3-dionate] was obtained [65]. By using the "complexes as ligands" approach, the novel bimetallic complex

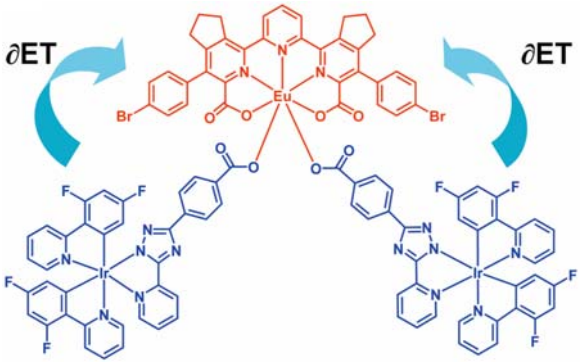

Fig. 28 The first example of sensitization of Eu^{III} emission through an iridium complex

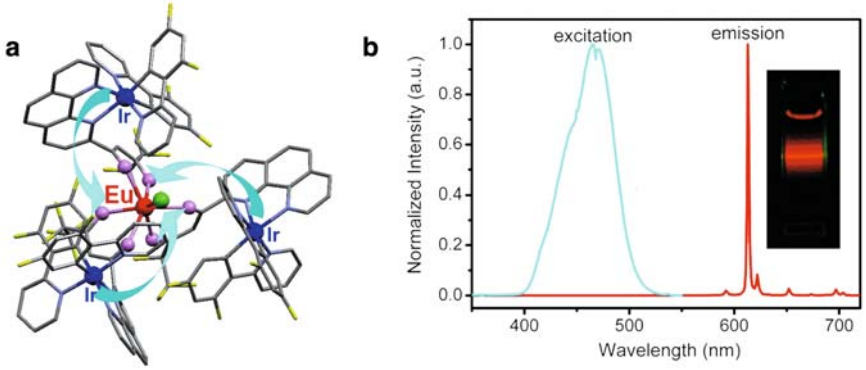

Fig. 29 (**a**) The crystal structure of "Ir_3Eu" assembly. (**b**) Pure-red emission of the "Ir_3Eu" assembly in EtOH (1×10^{-3} M) upon excitation of a 532-nm laser

$\{[(dfppy)_2Ir(\mu\text{-phen5f})]_3EuCl\}Cl_2$ was synthesized, and efficient pure-red luminescence from Eu^{III} was sensitized by ^{3}MLCT energy from the Ir^{III} moiety (Fig. 29). The excitation window can extend up to 530 nm due to the introduction of the *d*-block metal moiety, so this bimetallic complex can readily emit red light under sunlight irradiation.

As important phosphorescent materials, many Ir^{III} complexes with different energies of the lowest excited states have been extensively investigated by modifying cyclometalated ligands. This is a good strategy to seek more suitable Ir^{III} complexes to sensitize NIR lanthanide ions. Our research group has changed the cyclometalated ligand from dfppy to ppy to reduce the triplet energy level of the whole *d*-block complex-ligand and make it more suitable for NIR Ln^{III}. Another Ir^{III} complex $Ir(ppy)_2(phen5f)$ was introduced to form Ir_2Ln (Ln = Nd, Yb, Er) arrays. NIR emission upon photoexcitation of the Ir^{III}-centered antenna

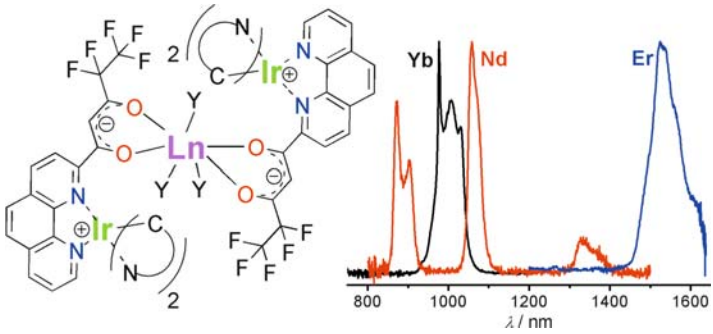

Fig. 30 Structures of Ir_2Ln (Ln = Nd, Yb, Er) arrays and corresponding near-infrared emissions. C^N denotes cyclometalated ligand ppy, and Y denotes bidentate nitrate anion

chromophore was successfully obtained (Fig. 30) [121]. An article involving sensitized NIR emission from Yb via direct energy transfer from Ir in a heterometallic neutral complex was published at virtually the same time by De Cola et al. [66].

4.4 Sensor Applications

Photoluminescent materials in which luminescence output can be modified by interaction with a substrate are being extensively investigated for use as sensors. Luminescent Ir complexes have been used as oxygen sensors, homocysteine sensors, metal cation sensors, and volatile organic compound sensors because of their rich photophysical properties.

4.4.1 Oxygen Sensor

Luminescence-based oxygen sensors work on the principle of luminescence quenching by oxygen; the excited luminophore enables efficient energy transfer to the triplet ground state of molecular oxygen, resulting in a nonradiative luminophore and formation of singlet oxygen [122]. Ir complexes are attractive candidates as novel luminescence-based oxygen-sensing materials (primarily because Ir complexes are the best known luminescent metal complexes). They can be excited with visible light, and their excited state is mainly a mixed ^{3}MLCT and ^{3}LC level, which is prone to quenching by molecular oxygen.

The first example of an Ir complex-based oxygen sensor was reported by Donckt et al. in 1994 [123]. They embedded *fac*-**1** in polystyrene and studied the luminescence properties of the system for use as an oxygen sensor to avoid self-quenching of *fac*-**1** at higher concentration. In 1996, DiMarco et al. [124] reported another Ir complex $[Ir(ppy)_2(dpt\text{-}NH_2)](PF_6)$ (where dpt-NH_2 = 4-amino-3,5-di-2-pyridyl-4*H*-l,2,4-triazole), immobilized in a polymerized poly-(ethyleneglycol) ethyl ether

methacrylate (pPEGMA) matrix. The system exhibited excellent properties as a quenchometric oxygen sensor (e.g., linear Stern–Volmer plot, photostability, thermal stability, and reproducibility). They extended their study in 1998 and reported the oxygen sensor ability of a series of mononuclear and dinuclear cyclometalated Ir complexes immobilized in pPEGMA matrixes [125]. The sensitivity and response of the sensor system was affected not only by the lifetime of the Ir complex and the permeability of matrices, but also by the size and charge of the Ir complex. This is important for the design of new solid-state luminescent sensors with improved performance. Efforts were subsequently focused on covalently binding the luminophore to different polymeric hosts, as well as adjusting the structure of the Ir complex [11, 68, 70, 122, 126].

4.4.2 Homocysteine Sensor

Homocysteine has a unique role within physiologic matrices because it is an important amino acid containing a free thiol moiety. Detection of homocysteine from other amino acids is therefore important. A selective phosphorescence chemosensor for this aim was developed based on the reaction shown in Fig. 31 [127]. Upon addition of homocysteine to a semiaqueous solution of **61**, a color change from orange to yellow and a luminescent variation from deep red to green were evident to the naked eye. This can be attributed to formation of a thiazinane group by selective reaction of the aldehyde group of **61** with homocysteine.

4.4.3 Metal Cation Sensor

Binding an appropriate metal ion to the ligand may lead to sufficient changes in luminescence because the photophysical properties of the Ir complex are influenced by the structure or surrounding environment of the organic ligands. In 2006, Ho et al. [128] presented a novel system in which an azacrown receptor was attached to the pyridyl pyrazolate chelate of a heteroleptic Ir complex. Photophysical study showed that phosphorescence was gradually blue-shifted from 560 to 520 nm, and was accompanied by an increase of emission intensity upon addition of Ca^{2+}, which made the complex a highly sensitive phosphorescence probe. In 2007, Schmittel

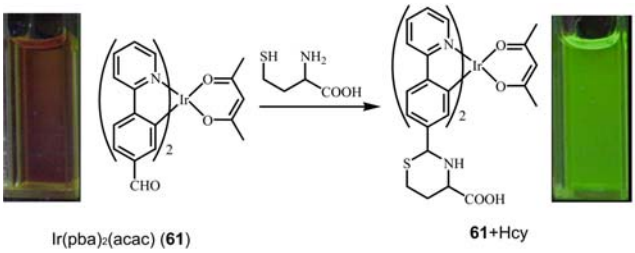

Ir(pba)2(acac) (**61**) **61**+Hcy

Fig. 31 Luminescent iridium complex-based sensor for homocysteine

et al. [129] synthesized **62** by introducing a crown group. The complex exhibited selective binding properties toward Ag^+ and Hg^{2+} in aqueous media, accompanied by characteristic luminescence responses. As shown in Fig. 32, luminescence was enhanced by >10 times in the presence of excess Ag^+; this is because the diimine ligand becomes an increasingly better acceptor by binding Ag^+. The emission quenched about 80% upon addition of Hg^{2+}, which may be explained by competition between emission-enhancing effects (decrease of the electron-donating ability of nitrogen upon Hg^{2+} binding) and the electron- or energy transfer-quenching effects of unbound Hg^{2+} ions. Ho et al. [130] demonstrated the concept of Pb^{2+} cation-sensing using the emissive Ir complex, which is based on the associated reduction of phosphorescence at room temperature upon chelate interaction between the Ir complex and metal analyte.

4.4.4 Acetonitrile or Propiononitrile Vapor Sensor

Sensor applications involving significant color and/or luminescence efficiency tuning mentioned above are usually based on structural or coordinated environment changes in the cyclometalated or ancillary ligand. We recently found the first example of an Ir complex PIrqnx (**63**) having a unique, fast vapochromic and vapoluminescent behavior towards acetonitrile or propiononitrile vapor based on molecular packing transformation (Fig. 33) [131]. Complex **63** exists as black

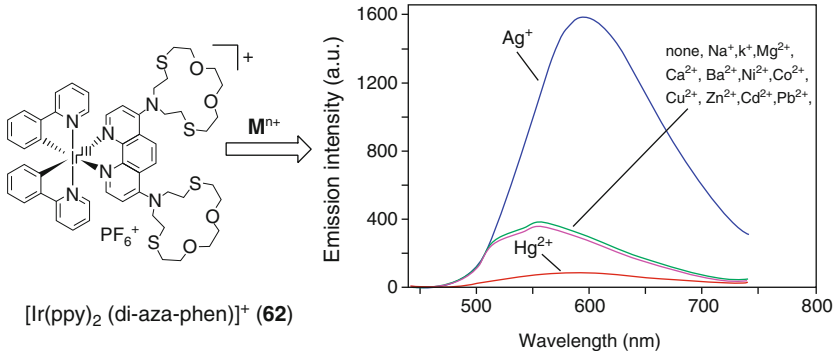

Fig. 32 Iridium-based chemosensors for Ag^+ and Hg^{2+} in aqueous media

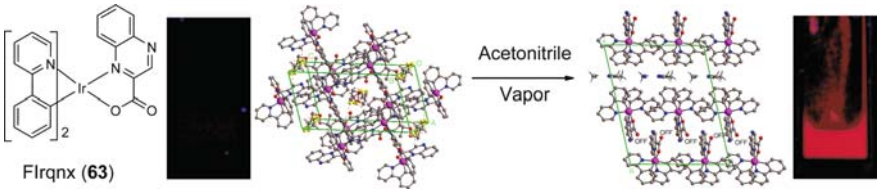

Fig. 33 An iridium complex that can detect acetonitrile or propiononitrile vapor

and red forms (visible to the naked eye) in the solid state. The black form can be transformed to the red form upon exposure to acetonitrile or propiononitrile vapor, but no response was observed when it was exposed to other volatile organic compounds. Crystallographic and DFT studies indicated that the black form adsorbed acetonitrile vapor first because of a porous packing structure, then the red form was formed with different color and luminescence properties induced by weak intermolecular interactions (e.g., hydrogen bonding, π–π interactions).

5 Summaries and Outlook

As can be seen from the evolution of Ir complexes discussed in this chapter, chemical syntheses are carried out to coordinate different ligand structures to the metal center to control the excited state. Ir complexes are therefore tailored to express specific luminescent properties, and are being explored for many applications (e.g., OLEDs, biological labeling reagents, chemosensors). And with the efforts of research groups investigating luminescent Ir complexes, we believe the future is very bright indeed.

Acknowledgments The authors acknowledge financial support from the National Basic Research Program of China (2006CB601103) and the National Natural Science Foundation of China (20021101, 20423005, 20471004, 50372002, and 20671006).

References

1. Baldo MA, O'Brien DF, You Y, Shoustikov A, Sibley S, Thompson ME, Forrest SR (1998) Nature 395:151–154
2. Baldo MA, Lamansky S, Burrows PE, Thompson ME, Forrest SR (1999) Appl Phys Lett 75:4–6
3. Watts RJ, Houten JV (1974) J Am Chem Soc 96:4334–4335
4. Dedeian K, Djurovich PI, Garces FO, Carlson G, Watts RJ (1991) Inorg Chem 30:1685–1687
5. Lowry MS, Goldsmiths JI, Slinker JD, Rohl R, Pascal RA, Malliaras GG, Bernhard S (2005) Chem Mater 17:5712–5719
6. Lamansky S, Djurovich P, Murphy D, Abdel-Razzaq F, Lee HE, Adachi C, Burrows PE, Forrest SR, Thompson ME (2001) J Am Chem Soc 123:4304–4312
7. Zhou GJ, Wong WY, Yao B, Xie ZY, Wang LX (2007) Angew Chem Int Ed 46:1149–1151
8. Tsuboyama A, Iwawaki H, Furugori M, Mukaide T, Kamatani J, Igawa S, Moriyama T, Miura S, Takiguchi T, Okada S, Hoshino M, Ueno K (2003) J Am Chem Soc 125:12971–12979
9. Okada S, Okinaka K, Iwawaki H, Furugori M, Hashimoto M, Mukaide T, Kamatani J, Igawa S, Tsuboyama A, Takiguchi T, Ueno K (2005) Dalton Trans:1583–1590
10. Adachi C, Baldo MA, Forrest SR, Thompson ME (2000) Appl Phys Lett 77:904–906
11. Amao Y, Ishikawa Y, Okura I (2001) Anal Chim Acta 445:177–182

12. Blumstengel S, Meinardi F, Tubino R, Gurioli M, Jandke M, Strohriegl P (2001) J Chem Phys 115:3249–3255
13. Grushin VV, Herron N, LeCloux DD, Marshall WJ, Petrov VA, Wang Y (2001) Chem Commun 1494–1495
14. Adamovich V, Brooks J, Tamayo A, Alexander AM, Djurovich PI, D'Andrade BW, Adachi C, Forrest SR, Thompson ME (2002) New J Chem 26:1171–1178
15. Tamayo AB, Alleyne BD, Djurovich PI, Lamansky S, Tsyba I, Ho NN, Bau R, Thompson ME (2003) J Am Chem Soc 125:7377–7387
16. King KA, Spellane PJ, Watts RJ (1985) J Am Chem Soc 107:1431–1432
17. Colombo MG, Brunold TC, Riedener T, Gudel HU, Fortsch M, Burgi HB (1994) Inorg Chem 33:545–550
18. Brunner K, van Dijken A, Borner H, Bastiaansen J, Kiggen NMM, Langeveld BMW (2004) J Am Chem Soc 126:6035–6042
19. Adachi C, Baldo MA, Forrest SR, Lamansky S, Thompson ME, Kwong RC (2001) Appl Phys Lett 78:1622–1624
20. Adachi C, Baldo MA, Thompson ME, Forrest SR (2001) J Appl Phys 90:5048–5051
21. Adachi C, Kwong RC, Djurovich P, Adamovich V, Baldo MA, Thompson ME, Forrest SR (2001) Appl Phys Lett 79:2082–2084
22. Ikai M, Tokito S, Sakamoto Y, Suzuki T, Taga Y (2001) Appl Phys Lett 79:156–158
23. Lamansky S, Djurovich P, Murphy D, Abdel-Razzaq F, Kwong R, Tsyba I, Bortz M, Mui B, Bau R, Thompson ME (2001) Inorg Chem 40:1704–1711
24. Duan JP, Sun PP, Cheng CH (2003) Adv Mater 15:224–228
25. Holmes RJ, D'Andrade BW, Forrest SR, Ren X, Li J, Thompson ME (2003) Appl Phys Lett 83:3818–3820
26. Su YJ, Huang HL, Li CL, Chien CH, Tao YT, Chou PT, Datta S, Liu RS (2003) Adv Mater 15:884–888
27. Tokito S, Iijima T, Tsuzuki T, Sato F (2003) Appl Phys Lett 83:2459–2461
28. Coppo P, Plummer EA, De Cola L (2004) Chem Commun 1774–1775
29. Wilkinson AJ, Puschmann H, Howard JAK, Foster CE, Williams JAG (2006) Inorg Chem 45:8685–8699
30. Wilkinson AJ, Goeta AE, Foster CE, Williams JAG (2004) Inorg Chem 43:6513–6515
31. Williams JAG, Wilkinson AJ, Whittle VL (2008) Dalton Trans 2081–2099
32. Neve F, Crispini A (2000) Eur J Inorg Chem 1039–1043
33. Lo KKW, Ng DCM, Chung CK (2001) Organometallics 20:4999–5001
34. Lo KKW, Chung CK, Ng DCM, Zhu NY (2002) New J Chem 26:81–88
35. Lo KKW, Chung CK, Lee TKM, Lui LH, Tsang KHK, Zhu NY (2003) Inorg Chem 42:6886–6897
36. Lo KKW, Chung CK, Zhu NY (2003) Chem Eur J 9:475–483
37. Colombo MG, Gudel HU (1993) Inorg Chem 32:3081–3087
38. Colombo MG, Hauser A, Gudel HU (1993) Inorg Chem 32:3088–3092
39. Ohsawa Y, Sprouse S, King KA, Dearmond MK, Hanck KW, Watts RJ (1987) J Phys Chem 91:1047–1054
40. Maestri M, Sandrini D, Balzani V, Maeder U, Vonzelewsky A (1987) Inorg Chem 26:1323–1327
41. Nazeeruddin MK, Humphry-Baker R, Berner D, Rivier S, Zuppiroli L, Graetzel M (2003) J Am Chem Soc 125:8790–8797
42. Whittle VL, Williams JAG (2008) Inorg Chem 47:6596–6607
43. Goodall W, Wild K, Arm KJ, Williams JAG (2002) J Chem Soc Perkin Trans 2:1669–1681
44. Leslie W, Batsanov AS, Howard JAK, Williams JAG (2004) Dalton Trans 623–631
45. Inomata H, Goushi K, Masuko T, Konno T, Imai T, Sasabe H, Brown JJ, Adachi C (2004) Chem Mater 16:1285–1291
46. Paulose B, Rayabarapu DK, Duan JP, Cheng CH (2004) Adv Mater 16:2003–2007

47. Rayabarapu DK, Paulose B, Duan JP, Cheng CH (2005) Adv Mater 17:349–353
48. Yeh SJ, Wu MF, Chen CT, Song YH, Chi Y, Ho MH, Hsu SF, Chen CH (2005) Adv Mater 17:285–289
49. Guan M, Chen ZQ, Bian ZQ, Liu ZW, Gong ZL, Baik W, Lee HJ, Huang CH (2006) Org Electron 7:330–336
50. Tsuzuki T, Tokito S (2007) Adv Mater 19:276–280
51. Ho CL, Wong WY, Gao ZQ, Chen CH, Cheah KW, Yao B, Xie ZY, Wang Q, Ma DG, Wang LA, Yu XM, Kwok HS, Lin ZY (2008) Adv Funct Mater 18:319–331
52. Bolink HJ, Cappelli L, Coronado E, Gratzel M, Orti E, Costa RD, Viruela PM, Nazeeruddin MK (2006) J Am Chem Soc 128:14786–14787
53. Bolink HJ, Cappelli L, Coronado E, Parham A, Stossel P (2006) Chem Mater 18:2778–2780
54. Chen FC, Yang Y, Pei Q (2002) Appl Phys Lett 81:4278–4280
55. Su HC, Chen HF, Fang FC, Liu CC, Wu CC, Wong KT, Liu YH, Peng SM (2008) J Am Chem Soc 130:3413–3419
56. Zeng XS, Tavasli M, Perepichka IE, Batsanov AS, Bryce MR, Chiang CJ, Rothe C, Monkman AP (2008) Chem Eur J 14:933–943
57. Bolink HJ, Cappelli L, Cheylan S, Coronado E, Costa RD, Lardies N, Nazeeruddin MK, Orti E (2007) J Mater Chem 17:5032–5041
58. Dragonetti C, Falciola L, Mussini P, Righetto S, Roberto D, Ugo R, Valore A, De Angelis F, Fantacci S, Sgamellotti A, Ramon M, Muccini M (2007) Inorg Chem 46:8533–8547
59. Tamayo AB, Garon S, Sajoto T, Djurovich PI, Tsyba IM, Bau R, Thompson ME (2005) Inorg Chem 44:8723–8732
60. Nazeeruddin MK, Wegh RT, Zhou Z, Klein C, Wang Q, De Angelis F, Fantacci S, Gratzel M (2006) Inorg Chem 45:9245–9250
61. Lo KKW, Zhang KY, Leung SK, Tang MC (2008) Angew Chem Int Ed 47:2213–2216
62. Lo KKW, Zhang KY, Chung CK, Kwok KY (2007) Chem Eur J 13:7110–7120
63. Lo KKW, Chung CK, Zhu NY (2006) Chem Eur J 12:1500–1512
64. Lo KKW, Hui WK, Chung CK, Tsang KHK, Ng DCM, Zhu NY, Cheung KK (2005) Coord Chem Rev 249:1434–1450
65. Chen FF, Bian ZQ, Liu ZW, Nie DB, Chen ZQ, Huang CH (2008) Inorg Chem 47:2507–2513
66. Mehlstaubl M, Kottas GS, Colella S, De Cola L (2008) Dalton Trans 2385–2388
67. Coppo P, Duati M, Kozhevnikov VN, Hofstraat JW, De Cola L (2005) Angew Chem Int Ed 44:1806–1810
68. DeRosa MC, Hodgson DJ, Enright GD, Dawson B, Evans CEB, Crutchley RJ (2004) J Am Chem Soc 126:7619–7626
69. Borisov SM, Klimant I (2007) Anal Chem 79:7501–7509
70. Fernandez-Sanchez JF, Roth T, Cannas R, Nazeeruddin MK, Spichiger S, Graetzel M, Spichiger-Keller UE (2007) Talanta 71:242–250
71. Medina-Castillo AL, Fernandez-Sanchez JF, Klein C, Nazeeruddin MK, Segura-Carretero A, Fernandez-Gutierrez A, Graetzel M, Spichiger-Keller UE (2007) Analyst 132:929–936
72. Lo SC, Male NAH, Markham JPJ, Magennis SW, Burn PL, Salata OV, Samuel IDW (2002) Adv Mater 14:975–979
73. Markham JPJ, Samuel IDW, Lo SC, Burn PL, Weiter M, Bassler H (2004) J Appl Phys 95:438–445
74. Lo SC, Richards GJ, Markham JPJ, Namdas EB, Sharma S, Burn PL, Samuel IDW (2005) Adv Funct Mater 15:1451–1458
75. Zhou GJ, Wong WY, Yao B, Xie Z, Wang L (2008) J Mater Chem 18:1799–1809
76. Li XH, Chen Z, Zhao Q, Shen L, Li FY, Yi T, Cao Y, Huang CH (2007) Inorg Chem 46:5518–5527
77. Hwang SH, Shreiner CD, Moorefield CN, Newkome GR (2007) New J Chem 31:1192–1217
78. Lo SC, Burn PL (2007) Chem Rev 107:1097–1116
79. Nonoyama M (1974) Bull Chem Soc Jpn 47:767–768

80. Li J, Djurovich PI, Alleyne BD, Tsyba I, Ho NN, Bau R, Thompson ME (2004) Polyhedron 23:419–428
81. Song YH, Yeh SJ, Chen CT, Chi Y, Liu CS, Yu JK, Hu YH, Chou PT, Peng SM, Lee GH (2004) Adv Funct Mater 14:1221
82. Chen XW, Liao JL, Liang YM, Ahmed MO, Tseng HE, Chen SA (2003) J Am Chem Soc 125:636–637
83. Nonoyama M (1974) J Organomet Chem 82:271–276
84. Zhao Q, Liu SJ, Shi M, Wang CM, Yu MX, Li L, Li FY, Yi T, Huang CH (2006) Inorg Chem 45:6152–6160
85. Di Censo D, Fantacci S, De Angelis F, Klein C, Evans N, Kalyanasundaram K, Bolink HJ, Gratzel M, Nazeeruddin MK (2008) Inorg Chem 47:980–989
86. Ayala NP, Flynn CM, Sacksteder L, Demas JN, Degraff BA (1990) J Am Chem Soc 112:3837–3844
87. Baranoff E, Collin JP, Flamigni L, Sauvage JP (2004) Chem Soc Rev 33:147–155
88. Douglas B, McDaniel D, Alexander J (1994) Concepts and models in inorganic chemistry, 3rd edn. Wiley, New York
89. Liu ZW, Nie DB, Bian ZQ, Chen FF, Lou B, Bian J, Huang CH (2008) ChemPhysChem 9:634–640
90. You Y, Seo J, Kim SH, Kim KS, Ahn TK, Kim D, Park SY (2008) Inorg Chem 47:1476–1487
91. You Y, Kim KS, Ahn TK, Kim D, Park SY (2007) J Phys Chem C 111:4052–4060
92. You YM, Park SY (2005) J Am Chem Soc 127:12438–12439
93. Hay PJ (2002) J Phys Chem A 106:1634–1641
94. De Angelis F, Fantacci S, Evans N, Klein C, Zakeeruddin SM, Moser JE, Kalyanasundaram K, Bolink HJ, Gratzel M, Nazeeruddin MK (2007) Inorg Chem 46:5989–6001
95. Holmes RJ, Forrest SR, Tung YJ, Kwong RC, Brown JJ, Garon S, Thompson ME (2003) Appl Phys Lett 82:2422–2424
96. Lin JJ, Liao WS, Huang HJ, Wu FI, Cheng CH (2008) Adv Funct Mater 18:485–491
97. Su SJ, Sasabe H, Takeda T, Kido J (2008) Chem Mater 20:1691–1693
98. Williams EL, Li J, Jabbour GE (2006) Appl Phys Lett 89:083506
99. D'Andrade BW, Thompson ME, Forrest SR (2002) Adv Mater 14:147–151
100. D'Andrade BW, Holmes RJ, Forrest SR (2004) Adv Mater 16:624–628
101. Kwong RC, Lamansky S, Thompson ME (2000) Adv Mater 12:1134–1138
102. Liu ZW, Bian ZQ, Hao F, Nie DB, Ding F, Chen ZQ, Huang CH (2009) Org Electron. doi:10.1016/j.orgel.2008.11.013
103. Gong JR, Wan LJ, Lei SB, Bai CL, Zhang XH, Lee ST (2005) J Phys Chem B 109:1675–1682
104. Song YH, Yeh SJ, Chen CT, Chi Y, Liu CS, Yu JK, Hu YH, Chou PT, Peng SM, Lee GH (2004) Adv Funct Mater 14:1221–1226
105. Wang Y, Herron N, Grushin VV, LeCloux D, Petrov V (2001) Appl Phys Lett 79:449–451
106. Liu ZW, Guan M, Bian ZQ, Nie DB, Gong ZL, Li ZB, Huang CH (2006) Adv Funct Mater 16:1441–1448
107. Liu ZW, Bian ZQ, Ming L, Ding F, Shen HY, Nie DB, Huang CH (2008) Org Electron 9:171–182
108. Slinker JD, Koh CY, Malliaras GG, Lowry MS, Bernhard S (2005) Appl Phys Lett 86:173506
109. Slinker JD, Gorodetsky AA, Lowry MS, Wang JJ, Parker S, Rohl R, Bernhard S, Malliaras GG (2004) J Am Chem Soc 126:2763–2767
110. Lowry MS, Goldsmith JI, Slinker JD, Rohl R, Pascal RA, Malliaras GG, Bernhard S (2005) Chem Mater 17:5712–5719
111. Yu MX, Zhao Q, Shi LX, Li FY, Zhou ZG, Yang H, Yia T, Huang CH (2008) Chem Commun 2115–2117

112. Adachi C, Baldo MA, Forrest SR (2000) J Appl Phys 87:8049–8055
113. Hong ZR, Liang CJ, Li RG, Li WL, Zhao D, Fan D, Wang DY, Chu B, Zang FX, Hong LS, Lee ST (2001) Adv Mater 13:1241–1245
114. Sun M, Xin H, Wang KZ, Zhang YA, Jin LP, Huang CH (2003) Chem Commun 702–703
115. Liang FS, Zhou QG, Cheng YX, Wang LX, Ma DG, Jing XB, Wang FS (2003) Chem Mater 15:1935–1937
116. Kang TS, Harrison BS, Bouguettaya M, Foley TJ, Boncella JM, Schanze KS, Reynolds JR (2003) Adv Funct Mater 13:205–210
117. Kawamura Y, Wada Y, Hasegawa Y, Iwamuro M, Kitamura T, Yanagida S (1999) Appl Phys Lett 74:3245–3247
118. Motson GR, Fleming JS, Brooker S (2004) Potential applications for the use of lanthanide complexes as luminescent biolabels. In: Advances in inorganic chemistry: including bio-inorganic studies, vol 55. Academic, London, pp 361–432
119. Bunzli JCG, Piguet C (2005) Chem Soc Rev 34:1048–1077
120. Werts MHV, Jukes RTF, Verhoeven JW (2002) Phys Chem Chem Phys 4:1542–1548
121. Chen FF, Bian ZQ, Lou B, Ma E, Liu ZW, Nie DB, Chen ZQ, Bian J, Chen ZN, Huang CH (2008) Dalton Trans 41:5577–5583
122. DeRosa MC, Mosher PJ, Evans CEB, Crutchley RJ (2003) Macromol Symp 196:235–248
123. Vanderdonckt E, Camerman B, Hendrick F, Herne R, Vandeloise R (1994) Bull Soc Chim Belg 103:207–211
124. DiMarco G, Lanza M, Pieruccini M, Campagna S (1996) Adv Mater 8:576–580
125. Di Marco G, Lanza M, Mamo A, Stefio I, Di Pietro C, Romeo G, Campagna S (1998) Anal Chem 70:5019–5023
126. DeRosa MC, Mosher PJ, Yap GPA, Focsaneanu KS, Crutchley RJ, Evans CEB (2003) Inorg Chem 42:4864–4872
127. Chen HL, Zhao Q, Wu YB, Li FY, Yang H, Yi T, Huang CH (2007) Inorg Chem 46:11075–11081
128. Ho ML, Hwang FM, Chen PN, Hu YH, Cheng YM, Chen KS, Lee GH, Chi Y, Chou PT (2006) Org Biomol Chem 4:98–103
129. Schmittel M, Lin HW (2007) Inorg Chem 46:9139–9145
130. Ho ML, Cheng YM, Wu LC, Chou PT, Lee GH, Hsu FC, Chi Y (2007) Polyhedron 26:4886–4892
131. Liu ZW, Bian ZQ, Bian J, Li ZD, Nie DB, Huang CH (2008) Inorg Chem 47:8025–8030